Journal of Nonlinear Optical Physics & Materials
Vol. 9, No. 1 (2000) 105–116

PERCOLATION AND FRACTAL COMPOSITES: OPTICAL STUDIES

S. DUCOURTIEUX, S. GRÉSILLON, A. C. BOCCARA, J. C. RIVOAL,
X. QUELIN* and P. GADENNE*
Université P. et M. Curie, Laboratoire d'Optique Physique,
ESPCI, 75231 Paris, France
**LMOV, CNRS UMR 8634, Université de Versailles Saint-Quentin,*
78035 Versailles, France

V. P. DRACHEV†, W. D. BRAGG, V. P. SAFONOV‡, V. A. PODOLSKIY,
Z. C. YING, R. L. ARMSTRONG and VLADIMIR M. SHALAEV
Department of Physics, New Mexico State University, Las Cruces, NM 88003
†*Institute of Semiconductor Physics, Novosibirsk 630090, Russia*
‡*Institute of Automation and Electrometry, Novosibirsk 630090, Russia*

Received 29 November 1999

Local field distributions are studied in random metal–dielectric films near percolation (percolation films) and fractal aggregates of colloidal particles. For both systems, it is shown that optical excitations are localized in small nanometer-scale areas, "hot spots," where the local fields are much larger than the field of an incident electromagnetic wave. The large local fields result in giant enhancement of various optical phenomena. The surface-enhanced white-light generation and second-harmonic generation have been obtained in percolation films. For fractal aggregates of silver particles, a giant effect of *local* optical activity has been observed. The effect is due to surface-plasmon excitations localized on chiral-active particle configurations in fractals.

1. Introduction

Metal–dielectric composites, such as fractal aggregates of metal particles and semicontinuous metal films, have attracted much attention because their optical properties can be unique and significantly different from the optical properties of the bulk components forming the composite.[1–8]

Because of the special geometrical properties, optical excitations associated with surface plasmons tend to be localized in both type of nanostructured composites, fractal aggregates and metal–dielectric films near percolation (referred also to as percolation films).[8] In fractals, localization occurs due to their scale-invariant morphology which does not sustain propagating waves typical for translationally invariant systems. Percolation films, although homogeneous on the macroscopical scale, can be thought of as a collection of fractal metal clusters (in a dielectric host) of different sizes, from very small ones up to the "infinite" percolation cluster spanning

over the entire system.[9] As shown in Refs. 10 and 11 localization of surface plasmons in percolation films can be interpreted as a special type of Anderson localization occurring in disordered media.

The localization of optical excitations results in "hot spots," nanometer-size areas where the local field can significantly (by several orders of magnitude) exceed the applied field. The optical response of these hot spots, especially nonlinear one, can be dramatically enhanced. These hot spots can be studied by means of near-field optical microscopy, including its two important modifications, scanning near-field optical microscope (SNOM) and photon scanning tunneling microscope (PSTM).

In this paper we report results of our recent studies of percolation films (Sec. 2) and fractal aggregates of colloidal metal particles (Sec. 3).

2. Percolation Metal–Dielectric Films: Field Distribution and Enhanced Optical Nonlinearities

Semicontinuous metal films can be produced by thermal evaporation or sputtering of metal onto an insulating substrate. In the growing process, firstly, small metallic grains are formed on the substrate. A typical size a of a metal grain is about 5 nm to 50 nm. As the film grows, the metal filling factor increases and coalescence occurs, so that irregularly shaped clusters are formed on the substrate, eventually resulting in self-similar fractal structures. The concept of self-similarity plays an important role in the description of various properties of percolation systems.[9] The sizes of the fractal structures diverge in the vicinity of the percolation threshold, where an infinite cluster of metal is eventually formed, representing a continuous conducting path between the ends of a sample. At the percolation threshold the metal-insulator transition occurs in the system. At higher surface coverage, the film is mostly metallic, with voids of irregular shape. With further coverage increase the film becomes uniform.

Below we first outline our near-field optical studies of the local field distribution and then some enhanced optical nonlinearities in metal–dielectric percolation films.

2.1. *SNOM Imaging of Hot Spots*

We imaged the localized optical excitations in gold-on-glass percolation films, using scanning near-field optical microscopy (SNOM). The used SNOM probe is an apertureless tip made of a tungsten wire etched by electrochemical erosion.[12] The radius of curvature of the tip measured by scanning electron microscopy is about 10 nm, which provides very high spatial resolution needed to image the localized optical modes. The tip oscillates above a sample which is attached to an (x, y) horizontal piezoelectric stage. The tip is the bent end of the tungsten wire used as a cantilever connected to a twin-piezoelectric transducer that can excite it perpendicularly to the sample surface. The frequency of vibrations ($\sim$ 5 kHz) is close to the resonant frequency of the cantilever and its amplitude is about 50 nm. In the tapping mode the tip vibrates above the sample as in atomic force microscope (AFM). Detection

of the vibration amplitude is made by a double photodiode, detecting the lever-arm shadow in a laser diode probe beam. A feedback system, including a piezoelectric translator attached to the twin-piezoelectric transducer (needed for the tip vibrations), keeps constant the vibration amplitude during the sample scanning. The detection of the feedback voltage applied to the piezoelectric translator gives a topographical image of the surface, i.e. the AFM signal that can be taken simultaneously with the SNOM signal. A first microscope objective focuses the light of tunable cw Ti:Sapphire laser on the bottom surface of the sample. The signal collection is axially symmetric above the sample and it is made by a second microscope objective. The transmitted light passing through the microscope is then sent to a photomultiplier.

The tip vibration modulates the near-zone field on a sample surface and lock-in detection of the collected light at the tip's vibrational frequency allows one to detect the locally modulated field.[12] We note that the detected signal in such SNOM technique is proportional to the amplitude of the modulated local field rather than its intensity. In order to relate our results to other near-field measurements (where the local intensity is typically measured) the results shown below are squared to display the intensity of the detected signal.

For the visible and near-IR parts of the spectrum, the tungsten tip ($n \approx 3.5 + 2.8i$) does not have any resonances so that its polarizability is much less than the polarizability of the resonance-enhanced plasmon oscillations of the film. Because of this, perturbations in the field distribution introduced by the tip are relatively small. Our calculations of the tip perturbations, when it is modeled as a polarizable sphere, support this conclusion.[12]

Samples of semicontinuous metal films were prepared by depositing gold thin films on a glass substrate at room temperature under ultrahigh vacuum (10^{-9} Torr). In order to determine a closeness to the percolation threshold the resistivity and the deposited mass thickness were measured all along the film deposition. Optical reflection and transmission of the samples were also determined out of the vacuum chamber and compared with the well-known optical properties of percolation samples.[13] Transmission electron microscopy was performed afterwards by depositing the same film on a Cu grid covered by a very thin SiO_2 layer.

To process the SNOM data we used the following procedure. First, we removed a "pseudo-slop" in the optical data set, resulting from imperfections in the feedback loop (which also leads to slight change in the amplitude of the tip oscillations during the scanning) and, most importantly, from a drift of the whole set up. Such drift is typical for SNOM studies and often complicates interpretation of SNOM images. The drift was also seen in our AFM pictures of the samples which were known not to have any slop. To remove this pseudo-slop in the SNOM data, we first averaged the data for a number of cross section along the "x" and "y" axes and then, using the least-square fit, we defined the average slops in the "x" and "y" directions; these two average slops in turn allowed us to define the coordinates of the plane of inclination. To reveal the actual field distribution, this plane was brought back to

the $z = 0$ plane. The noise below zero appearing as a result of the used procedure was removed, which statistically does not affect the field distribution.

Then, as mentioned, we squared the detected signal in order to find the local field intensity. To find the local enhancement we normalized the local intensity by the mean of the detected signal squared that represents the intensity of the applied field. This is because the average local field on a percolation film, as shown in Ref. 10 is simply equal to the applied field, $\langle E \rangle = E_0$, so that when squared it gives the intensity of the applied field.

In Fig. 1, we show the near-field image of the local field distribution on the surface of a percolation gold-glass film at the light wavelength $\lambda = 800$ nm. In the SNOM image, resolution of one pixel is 16 nm, which is near the best resolution that can be achieved by SNOM. Our SNOM allows one to resolve even the most localized modes, with the localization radius of only 10 nm, i.e. about two orders of magnitude smaller than the optical wavelength.

One can see that, in accordance with theoretical predictions, there are sharp peaks representing the hot spots in the field distribution. We also note that although the detected field enhancement is of the order of 10^2 to 10^3, the actual enhancement right on the film surface (experienced, for example, by molecules adsorbed on the surface) is much stronger, and can reach the values between 10^4 and 10^5, as shown in Ref. 10. The decrease in the observed enhancement occurs because a signal

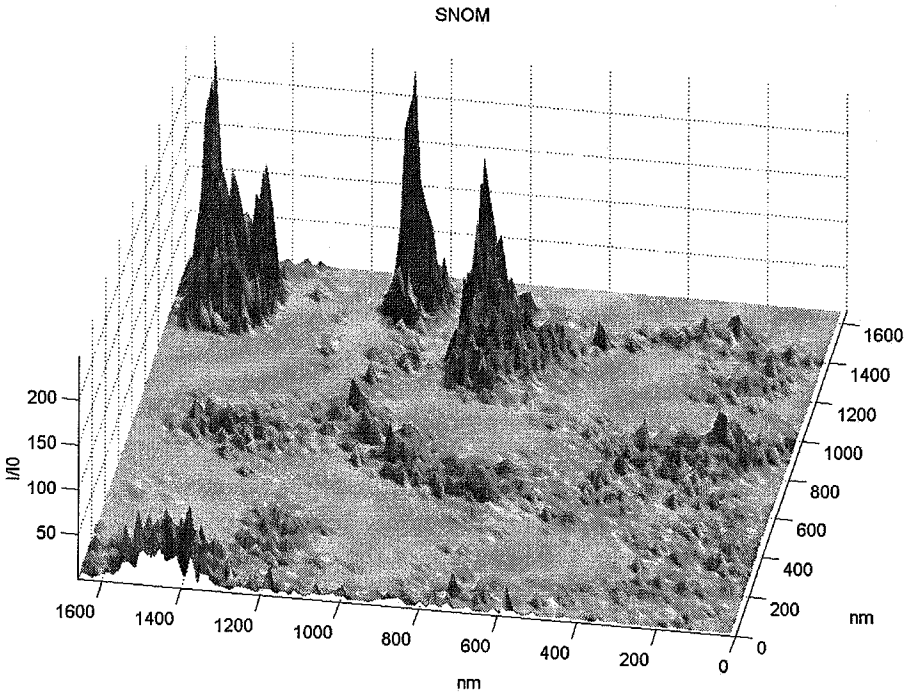

Fig. 1. SNOM images of the localized optical excitations in a percolation gold-on-glass film.

detected by the SNOM oscillating tip is averaged over all heights of the tip, from 0 nm to 100 nm, which is equivalent to the averaging over the period of oscillations.

To summarize this part, we note that in agreement with theoretical predictions, our SNOM studies show that optical excitations on metal–dielectric films are localized; the smallest hot spots can be about 10 nm in size, with a very strong field enhancement in these areas.

2.2. *Surface-Enhanced Supercontinuum and Second Harmonic Generation*

Strongly enhanced local field in the hot spots can lead to giant enhancement of optical nonlinearities.[8] One of most important optical nonlinearities is the Kerr-type optical response given by a third-order optical susceptibility. The Kerr optical nonlinearity results in nonlinear corrections (proportional to the light intensity) in the refractive index and absorption coefficient. It is also responsible for the four-wave mixing.[14] The nonlinear correction to the refractive index, strongly enhanced in percolation films, may lead, in turn, to self-phase modulation of a laser beam and spectral continuum generation, which we consider below.

Spectral continuum (also referred to as supercontinuum) generation, discovered in 1970, has now been demonstrated in a wide variety of solids, liquids, and gases.[15] Self-phase modulation, four-wave mixing, and plasma production (for the short-wavelength part of the spectrum) are most commonly invoked to explain continuum generation. According to a theory of self-phase modulation, the frequency-relative shift is proportional to the rate of change of the laser-induced refractive index (from the optical Kerr effect), such that $\Delta n = n_2 I_0$, and it can be approximated as $\Delta\omega/\omega \equiv Q \approx \beta z n_2 I_0/(c\tau)$, where $I_0 = (n_0 c/2\pi)|E_0|^2$ is the pulse average intensity of the applied field of the amplitude E_0 and frequency ω, n_0 is the linear refractive index, τ is the pulse duration, z is the interaction length, c is the speed of light, and prefactor β depends on the pulse temporal envelope and is ~ 1. In terms of the third-order nonlinear susceptibility $\chi^{(3)}$ of a medium, $n_2 \approx (12\pi^2/n_0^2 c)\chi^{(3)}$ (for the complex nonlinear susceptibility, the real part of $\chi^{(3)}$ is responsible for n_2).

In Ref. 10 we predicted that optical nonlinearities are strongly enhanced in a metal–dielectric film near the percolation threshold. This enhancement is due to giant local-field fluctuations associated with excitation of the collective surface plasmon (sp) modes of a percolation metal film. In particular, the Kerr optical nonlinearity $\chi^{(3)}$ experiences strong enhancement by the factor $G_K = \langle|E|^2 E^2\rangle/|E_0|^2 E^2$, which can be very large. For gold semicontinuous films on a glass substrate, G_K is estimated as $\sim 10^5$ at $\lambda \sim 1$ μm.[10]

The value of the surface-enhanced $\chi^{(3)}$ can be measured using the four-wave mixing technique; for gold percolation films, it was measured to be in the range from $\sim 10^{-6}$ esu to $\sim 10^{-5}$ at $\lambda \approx 0.7$ μm.[4]

Spectral continuum generation from percolation gold-on-glass thin films is observed in our experiments as described below. The light incoming from a Ti/Sapphire

laser at $\lambda \sim 0.79$ μm and repetition rate of 76 MHz was focused on an area ~ 1 μm^2 on the surface of the film. The pulse had a duration $\tau \sim 200$ fs.

The white light generation was observed for energies as low as $\sim 10^{-11}$ J. Samples of percolation gold films were prepared by depositing gold thin films on a glass substrate at room temperature under ultrahigh vacuum (10^{-9} Torr), as described above.

Figure 2 shows the spectral dependence of the relative intensity for the generated continuum at different mass equivalent film thicknesses; the intensity of the used laser radiation at $\lambda = 0.79$ μm is given by $I \approx 10^9$ W/cm^2. In our experiments, the continuum was detected in a large spectral range, from approximately 370 nm to 660 nm, which corresponds to the apparatus cutoffs (so that the actual generated range could be significantly broader). The observed spectral distribution is relatively flat because the sp eigenmodes of a percolation metal film cover a large spectral interval that includes the visible and near infrared parts of the spectrum, leading to the surface-enhanced $\chi^{(3)}$ in this broad spectral interval.

Using the value $\chi^{(3)} \sim 10^{-5}$ esu for the nonlinear susceptibility of percolation gold films, we find that the nonlinear refraction factor is estimated as $n_2 \sim 10^{-7}$ cm^2/W. Using then the obtained value of n_2, we calculate that the factor Q becomes of the order of unity, as required for supercontinuum generation, at the laser intensity $I \sim 10^9$ W/cm^2. This is the same intensity as the one found in our experiments, and it is four to five orders of magnitude less than the one typically uses to obtain white-light generation in media with no surface enhancement.[15]

We can attribute this five-order-of-magnitude decrease in the intensity needed for supercontinuum generation (predicted by theory and obtained experimentally)

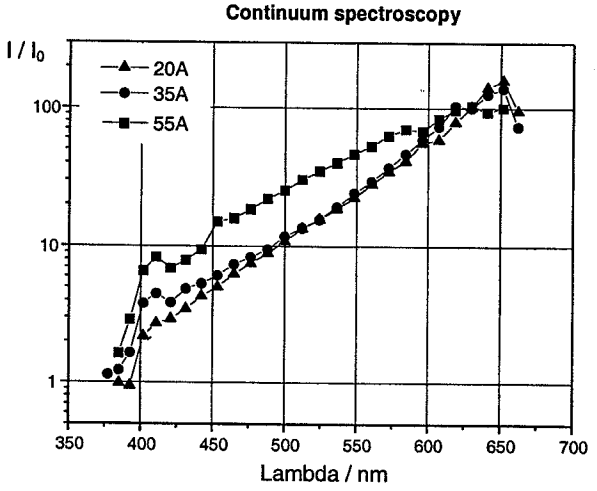

Fig. 2. The relative intensities of spectral continuum generated from random gold-on-glass film of different effective thicknesses, for the wavelength of the incident light $\lambda = 0.79$ μm, and the laser pulse intensity and duration $I = 10^9$ W/cm^2 and $\tau \approx 200$ fs, respectively. The percolation threshold corresponds to the mass equivalent thickness of 55 Å.

to the surface enhancement of the Kerr nonlinearity resulting from excitation of the collective sp modes of a percolation film.

The small peak near 400 nm in the spectral distribution in Fig. 2 is due to the surface-enhanced second-harmonic generation (SHG). This peak increases when approaching the percolation threshold corresponding to the mass equivalent thickness of 55 Å. Further studies of the SHG local distribution are currently in progress.

It is also important to note that local enhancements in the hot spots can be much larger than the average enhancements considered above. As follows from previous considerations,[10] the local field intensities are enhanced up to $|E/E_0|^2 \sim 10^4$, for gold semicontinuous films (for silver films it can be even larger). Therefore, for the Kerr-type nonlinearity, the local enhancement in the hot spots can be as large as 10^8. For the four-wave mixing, with the enhancement given by $G_{\mathrm{FWM}} \sim |G_K|^2$,[10] the local enhancement in the hot spots can be especially gigantic, up to 10^{16}. With such level of local enhancements, the nonlinear optical signals from single molecules and nanoparticles can be detected, which opens a fascinating possibility of local nonlinear spectroscopy with nanometer spatial resolution. These experimental studies are currently in progress.

Below we consider a novel effect of surface-enhanced *local* optical activity observed for fractal aggregates of metal nanoparticles. We note that similar effect is anticipated to exist in percolation films as well.

3. Fractal Aggregates of Metal Colloidal Particles: Giant Local Optical Activity

Recently, giant nonlinear optical activity in fractal silver aggregates has been reported,[16] which is one more among other intriguing optical phenomena predicted and obtained for fractal objects, including surface-plasmon-enhanced Raman scattering and giant optical nonlinearities.[8,17]

Natural optical activity has always been an active area of study in physics, chemistry, and biological sciences. Typically, this effect is observed for macroscopically large objects with unbalanced amount of left and right handed helical molecules. Optical activity, in particular, can be used to distinguish the enantiomers from each other, which is very important because the physiological and pharmacological effects of the enantiomers can be very different.[18]

In the case of fractal aggregates, gyrotropy studies can provide important information on chiral structure and polarization properties of fractal eigenmodes, which are localized in fractals and therefore sensitive to *local* arrangements of particles.[8,17,19] Colloidal particles forming fractal aggregates are typically 10 nm in size and the local resonating structures, "hot" spots, vary in size between tens to hundreds nanometers, i.e. can be comparable with the light wavelength. In this case, optical activity, which is a nonlocal effect and depends on light propagation, can be especially strong, for chiral arrangements of particles in fractals, such as twisted ladders and helical arrays. These structures are known to result in strong

optical activity, for example, in biological aggregates.[20] In metal fractals, the resonant structures of particles support collective surface-plasmon modes, with high resonance quality-factors. Thus, optical excitations of these chiral-active structures in fractals can also experience the resonant enhancement, resulting in giant surface-plasmon-enhanced optical activity.

It is interesting to note that for a macroscopic medium consisting of many fractals, or even for one large fractal, the macroscopic optical activity can be strongly decreased because contributions from local structures with different handedness cancel each other. However, locally, when one or few resonating chiral structures in fractals are probed, the optical activity can be very large. (In this case, a contribution to the local displacement current associated with the gyration vector can be comparable in magnitude with a contribution due to the dielectric tensor.) This *local surface-plasmon-enhanced* optical activity in fractals can be probed by means of near-field optical microscopy providing subwavelength resolution. Fractal aggregates can also be employed for the local surface-enhanced chiral spectroscopy of biological molecules deposited on the fractal surface.

Thus, a combination of two factors, large variety of local chiral-active structures in colloidal fractals supporting resonant plasmon oscillations and recent progress in near-field optical microscopy may serve as a precursor for developing a new field, surface-enhanced local chiral spectroscopy.

Optical activity phenomena are characterized by different responses to right and left circularly polarized light. It implies the difference in material attenuation (circular dichroism), refraction (circular birefringence), and scattering, for right and left circularly polarized light. The scattering optical activity is denoted as circular intensity differential scattering (CIDS).[21] All these effects depend on a certain relation between the chiral structure of material constituents and the handedness of an incident circularly polarized light. Scattering from optically active media, in general, changes a linear polarization of incident light to an elliptical polarization. Since it is difficult to make accurate ellipticity measurements with a divergent scattered light, it is often preferable to measure the circular intensity difference providing the same information on optical activity.[21] The CIDS is characterized by the dimensionless parameter: $\mathrm{CIDS} = (I_L - I_R)/(I_L + I_R) = -S_{14}/S_{11}$, where I_L and I_R are the scattered intensities from right and left circularly polarized incident light and S_{11}, S_{14} are elements of the Mueller scattering matrix,[22] characterizing the average intensity and optical activity, respectively.

The CIDS sensitivity to long-range structure of interacting dipoles can be a good indicator of spatial correlations in fractal systems.[8,23] The local fields in fractals induced by an external optical excitation consist of sharp singular peaks strongly fluctuating in space. Despite their singular structure on a subwavelength scale, for some modes, these fields can be delocalized over distances comparable with the wavelength. At any frequency, there coexist excitations (plasmons) with very different localization lengths, from the total size of the cluster to the size of a single particle. This pattern has been dubbed as inhomogeneous localization.[23]

Localization of plasmons in metallic fractal clusters was first observed in Ref. 24 and later in our experiments (performed at NMSU) with the use of photon scanning tunneling microscopy (PSTM), which is one of modification of near-field optical microscopy. Direct imaging of silver fractal surfaces shows a high sensitivity of the local-field intensity distribution to the wavelength, angle of incidence, and the light polarization when imaging with monochromatic, linearly polarized light.[24,25] The polarization dependence, in particular, illustrates strong local anisotropy of localized plasmon modes in fractals.

Here we report a locally huge CIDS of light by silver fractal aggregates, which proves that the surface-plasmon excitations in fractals can also be optically active. Using a PSTM technique, we studied the spatial distribution of the CIDS parameter, directly related to the local chiral structure of the sample. Locally, the CIDS parameter shows both strong wavelength dependence and extremely inhomogeneous spatial distribution, while the average (over large areas) CIDS is nearly zero. Thus, near-field CIDS measurements are well suited for studies of *local* optical activity on very small size scales.

Preparation of fractal aggregates and details on our PSTM apparatus are described elsewhere.[17,26] Fractal colloidal aggregates were mounted to the hypotenuse face of a 90° prism with index-matching fluid and illuminated by the evanescent field in the total internal reflection geometry. The illumination source was a helium-neon laser operating at 633 nm or a tunable diode laser (EOSI, 2010) operating between 790 and 820 nm. The polarization of the beam was controlled with a Glan–Thompson polarizer (New Focus, 5524) and a variable waveplate (New Focus, 5540) placed in the illumination beam before the sample prism. The local optical signal was collected through an uncoated optical fiber, which was sharpened to approximately 50 nm in radius at the tip using a fiber puller (Sutter Instruments P-2000). The separation between the tip and a sample was regulated using nonoptical shear-force feedback. Additionally, samples were scanned by rastering the tip in a constant plane above the sample without active feedback of the probe height. The comparison of the AFM and PSTM images obtained in the constant-height and the constant-plane modes demonstrated clearly the absence of topographically induced artifacts; in particular, the two types of PSTM images show approximately the same lateral resolution, bright spot size and optical contrast. Given this favorable comparison, nearly all measurements (phase dependence and wavelength dependence for four polarization states, totaling over 100 images) were performed in the constant-plane scanning mode to reduce tip wear and sample damage over the long experiment.

The scanning plane was slightly tilted, approximately 14°, with respect to the sample substrate, and the tip height changed from a minimum of about 100 nm to a maximum of about 2400 nm during a 10×10 μm^2 scan. Averaging of the sixteen images for different polarization states allowed us to determine the dependence of the detected intensity on the tip-sample separation. The detected signal is weakly dependent on the tip height and preserves a subwavelength lateral resolution even at relatively large distances, in agreement with observations by other authors.[27]

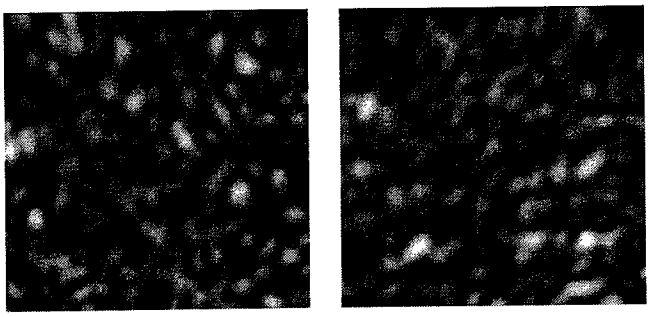

(a) right circular polarization (b) left circular polarization

Fig. 3. PSTM images of silver fractal aggregates with (a) right- and (b) left-circularly polarized incident light at 633 nm. Each image is 10 μm $\times$ 10 μm in size.

As shown in Ref. 28 the signal dependence on the tip–surface separation is very different for tips with large cone angles (typically 40°) and for sharper fiber tips (10°). Namely, a weak dependence is observed for sharper tips, that corresponds to our case, where the tip cone-angle was about 5°.

Figure 3 shows strong difference between local optical images for right and left circularly polarized incident light. The hot spots have different spatial distributions for the two polarizations.

Our experiments also show that there is strong wavelength dependence of the local CIDS parameter, which is different for different spatial locations. The local optical activity can be vary large and reach its maximum ($|S_{14}/S_{11}| \sim 1$), and it varies strongly with wavelength. In sharp contrast, the value of the CIDS parameter averaged over the whole sample 10×10 μm^2 is zero within experimental uncertainties for the whole spectral range studied in our experiments. These results point out that while locally there exist areas of strong preference for scattering of one circular polarization or another, the effect is much less or absent when averaged over macroscopic fractal samples. This brings about new avenues in the optical activity studies, which are opened up with the near-field scanning optical microscopy. The observed effect can also be employed for *local* surface-enhanced chiral spectroscopy of biological molecules deposited on the fractal surface.

We note that similar local optical activity is anticipated for metal–dielectric percolation films. These studies are currently in progress.

To summarize, localization of optical excitations in metal–dielectric composites leads to a palm of unusual optical effects which can find numerous applications. The optics of random media display a rich variety of effects some of which are hardly intuitive. Field localization of various sorts occur and recur in a wide gamut of disordered systems, most strikingly in those possessing dilational symmetry, leading to the enhancement of many optical phenomena, especially nonlinear processes. Making judicious use of these enhancement effects and of other aspects of the many complex resonances that distinguish these systems can lead to new and unexpected physics. When developed, in the fullness of time, these disordered materials may

attain a level of practical importance and versatility that might rival or surpass their geometrically ordered counterparts.

This work was supported by NSF under grant DMR-9810183, by ARO under grant DAAG55-98-1-0425, and by RFBR under grant 99-02-16670.

References

1. J. E. Sipe and R. W. Boyd, *Phys. Rev.* **B46**, 1614 (1992); R. J. Gehr, G. L. Fisher, R. W. Boyd and J. E. Sipe, *Phys. Rev.* **A53**, 2792 (1996); G. L. Fisher, R. W. Boyd, R. J. Gehr, S. A. Jenekhe, J. A. Osaheni, J. E. Sipe and L. A. Weller-Brophy, *Phys. Rev. Lett.* **74**, 1871 (1995); R. W. Boyd, R. J. Gehr, G. L. Fisher and J. E. Sipe, *Pure Appl. Opt.* **5**, 505 (1996).
2. D. J. Bergman and D. Stroud, in *Solid State Physics* **46**, 147 (Academic, 1992).
3. C. Flytzanis, *Prog. Opt.* **29**, 2539 (1992); D. Ricard, Ph. Roussignol and C. Flytzanis, *Opt. Lett.* **10**, 511 (1985); F. Hache, D. Ricard, C. Flytzanis and U. Kreibig, *Appl. Phys.* **A47**, 347 (1988).
4. H. B. Liao, R. F. Fiao, J. S. Fu, P. Yu, G. K. L. Wong and P. Sheng, *Appl. Phys. Lett.* **70**, 1 (1997); K. P. Yuen, M. F. Law, K. W. Yu and P. Sheng, *Phys. Rev.* **E56**, R1322 (1997); H. B. Liao, R. F. Xiao, J. S. Fu, H. Wang, K. S. Wong and G. K. L. Wong, *Opt. Lett.* **23**, 388 (1988); H. B. Liao, R. F. Xiao, H. Wang, K. S. Wong and G. K. L. Wong, *Appl. Phys. Lett.* **72**, 1817 (1998); W. M. V. Wan, H. C. Lee, P. M. Hui and K. W. Yu, *Phys. Rev.* **B54**, 3946 (1996); D. Stroud and P. M. Hui, *Phys. Rev.* **B37**, 8719 (1988).
5. U. Kreibig and M. Vollmer, *Optical Properties of Metal Clusters* (Springer-Verlag, Berlin Heidelberg, 1995).
6. *Electrical Transport and Optical Properties of Inhomogeneous Media*, eds. J. C. Garland and D. B. Tanner (AIP, New York, 1978); *Electrical Transport and Optical Properties of Inhomogeneous Media* (*ETOPIM* 2), eds. J. Laffait and D. B. Tanner, *Physica* **A157**, p. 1 (1988); *Electrical Transport and Optical Properties of Inhomogeneous Media* (*ETOPIM* 3), eds. W. L. Mochan and R. G. Barrera, North-Holland, Amsterdam (1994); *Physica* **A241**, Nos. 1–2, pp. 1–452 (1997); Proceedings of the Fourth International Conference on Electrical Transport and Optical Properties of Inhomogeneous Media (ETOPIM 4), eds. A. M. Dykhne, A. N. Lagarkov and A. K. Sarychev.
7. P. Gadenne, *Thin Solid Films* **57**, 77 (1979).
8. V. M. Shalaev, *Nonlinear Optics of Random Media: Fractal Composites and Metal–Dielectric Films* (Springer, Berlin, Heidelberg, STMP v. 158, 2000).
9. D. Stauffer and A. Aharony, *Introduction to Percolation Theory*, 2nd ed. (Taylor and Francis, Philadelphia, 1991).
10. V. M. Shalaev and A. K. Sarychev, *Phys. Rev.* **B57**, 13265 (1998); A. K. Sarychev and V. M. Shalaev, *Physica* **A266**, 115 (1999); A. K. Sarychev, V. A. Shubin and V. M. Shalaev, *Phys. Rev.* **E59**, 7239 (1999); F. Brouers, S. Blacher, A. N. Lagarkov, A. K. Sarychev, P. Gadenne and V. M. Shalaev, *Phys. Rev.* **B55**, 13234 (1997); V. A. Shubin, A. K. Sarychev and V. M. Shalaev, *Phys. Rev.* B, in press.
11. S. Gresillon, L. Aigouy, A. C. Boccara, J. C. Rivoal, X. Quelin, C. Desmarest, P. Gadenne, V. A. Shubin, A. K. Sarychev and V. M. Shalaev, *Phys. Rev. Lett.* **82**, 4520 (1999).
12. R. Bachelot *et al.*, *Appl. Opt.* **36**, 2160 (1997); P. Gleyzes *et al.*, *Appl. Phys. Lett.* **58**, 2989 (1991); A. Lahrech *et al.*, *Opt. Lett.* **21**, 1315 (1996).
13. P. Gadenne *et al.*, *J. Appl. Phys.* **66**, 3019 (1989); Y. Yagil *et al.*, *Phys. Rev.* **B46**,

14. R. W. Boyd, *Nonlinear Optics* (Academic, 1992).
15. R. R. Alfano and S. L. Shapiro, *Phys. Rev. Lett.* **24**, 592 (1970); G. Yang and Y. R. Sheng, *Opt. Lett.* **9**, 510 (1984); J. T. Manassah, M. A. Mustafa, R. R. Alfano and P. P. Ho, *IEEE J. Quantum Electron.* **224**, 197 (1986); P. B. Corkum, C. Rolland and T. Srinivasan-Rao, *Phys. Rev. Lett.* **57**, 2268 (1986); R. L. Fork, C. V. Shank, C. Hirliman, R. Yen and W. J. Tomlinson, *Opt. Lett.* **8**, 1 (1983).
16. V. P. Drachev *et al.*, *JETP Letts.* **68**, 651 (1998).
17. V. M. Shalaev, *Phys. Rep.* **272**, 61 (1996); V. P. Safonov *et al.*, *Phys. Rev. Lett.* **80**, 1102 (1998); W. Kim *et al.*, *Phys. Rev. Lett.* **82**, 4811 (1999).
18. M. Kauranen *et al.*, *J. Mod. Opt.* **45**, 403 (1998).
19. V. M. Shalaev and M. I. Stockman, *Sov. Phys. JETP* **65**, 287 (1987); V. A. Markel *et al.*, *Phys. Rev.* **B43**, 8183 (1991).
20. D. Keller *et al.*, *Biopolymers*, **24**, 783 (1985); S. B. Singham *et al.*, *J. Chem. Phys.* **85**(2), 763 (1986).
21. L. D. Barron, *Molecular Light Scattering and Optical Activity* (Cambridge University Press, 1982).
22. C. Bohren and D. Huffman, *Absorption and Scattering of Light by Small Particles* (John Wiley & Sons, 1983).
23. M. I. Stockman, *Phys. Rev. Lett.* **79**, 4562 (1997); M. I. Stockman, *Phys. Rev.* **E56**, 6494 (1997).
24. D. P. Tsai *et al.*, *Phys. Rev. Lett.* **72**, 4149 (1994); S. I. Bozhevolnyi *et al.*, *Phys. Rev.* **B58**, 11441 (1998).
25. V. A. Markel *et al.*, *Phys. Rev.* **B59**, 10903 (1999).
26. W. D. Bragg *et al.*, *J. Microscopy* **194**, 574 (1999).
27. P. Zhang, Ph.D. Thesis, Univ. of Toronto (1997).
28. S. I. Bozhevolnyi, *Phys. Rev.* **B54**, 8177 (1996).